Analytic approximations of 2 → 2 processes with massive internal particles

Davies, Joshua ; Mishima, Go ; Schönwald, Kay ; Steinhauser, Matthias

DOI: https://doi.org/10.1007/jhep06(2023)063

Published for SISSA by Springer

Received: February 9, 2023
Revised: March 28, 2023
Accepted: April 20, 2023
Published: June 13, 2023

Analytic approximations of $2 \to 2$ processes with massive internal particles

Joshua Davies,[a] **Go Mishima,**[b] **Kay Schönwald**[c] **and Matthias Steinhauser**[d]

[a] *Department of Physics and Astronomy, University of Sussex, Brighton BN1 9QH, U.K.*
[b] *Department of Physics, Tohoku University, Aobaku Aramaki Aza-aoba 6-3, 980-8578 Sendai, Japan*
[c] *Physik-Institut, Universität Zürich, Winterthurerstrasse 190, 8057 Zürich, Switzerland*
[d] *Institut für Theoretische Teilchenphysik, Karlsruhe Institute of Technology (KIT), Wolfgang-Gaede Straße 1, 76128 Karlsruhe, Germany*

E-mail: J.O.Davies@sussex.ac.uk, go.mishima.d2@tohoku.ac.jp, kay.schoenwald@physik.uzh.ch, matthias.steinhauser@kit.edu

Abstract: We consider two-loop corrections to $2 \to 2$ scattering processes with massive particles in the final state and massive particles in the loop. We discuss the combination of analytic expansions in the high-energy limit and for small Mandelstam variable t. For the example of double Higgs boson production we show that the whole phase space can be covered and time-consuming numerical integrations can be avoided.

Keywords: Higgs Production, Higgs Properties, Top Quark

ArXiv ePrint: 2302.01356

https://doi.org/10.1007/JHEP06(2023)063

JHEP06(2023)063

Contents

JHEP06(2023)063

1 Introduction

In many higher-order calculations of cross sections the virtual corrections are the bottleneck, particularly if they involve massive particles propagating in loops. A prominent example of such a process is Higgs boson pair production, where the real-radiation contribution with exact dependence on the top quark mass [1] was available long before the corresponding virtual corrections [2–4]. One of the reasons is certainly the enormous expressions which are present in intermediate stages of the calculation, and the complicated integrals which in general depend on several invariants. Often a purely numerical approach for the evaluation of the loop integrals is necessary, which comes with the well-known disadvantages of long run-times and reduced flexibility in the choice of values for parameters. In this paper we suggest an alternative approach for the computation of virtual loop integrals for $2 \to 2$ processes. It is based on the combination expansions in different kinematic regions.

We consider the scattering of two (massless) partons in the initial state with momenta q_1 and q_2 into two massive particles in the final state with momenta q_3 and q_4. It is convenient to introduce the Mandelstam variables as

$$s = (q_1 + q_2)^2\,, \qquad t = (q_1 + q_3)^2\,, \qquad u = (q_1 + q_4)^2\,, \tag{1.1}$$

where all momenta are incoming. Furthermore we have

$$q_1^2 = q_2^2 = 0\,, \qquad q_3^2 = m_X^2\,, \qquad q_4^2 = m_Y^2\,, \tag{1.2}$$

where in general m_X and m_Y are allowed to be different and the transverse momentum of the final-state particles is given by

$$p_T^2 = \frac{u\,t - m_X^2 m_Y^2}{s}\,. \tag{1.3}$$

For definiteness we will denote the internal mass by m_t, the top quark mass.

The computation of massive two-loop integrals with the kinematics described above is a difficult problem. Purely numerical approaches have been developed and applied to the processes $gg \to HH$, $gg \to ZZ$, $gg \to ZH$, $gg \to W^+W^-$ (see, e.g., refs. [2–7]). Usually these computations require a large amount of CPU time for a single phase space point. Furthermore, it is often necessary to fix numerical values for the top quark and Higgs boson masses at an early stage of the calculation. Thus a change of value or renormalization scheme makes it necessary to repeat a large part of the calculation.

In order to avoid the disadvantages of a purely numerical calculation a number of analytic approximation methods have been developed. Initially they have usually been applied to Higgs boson pair production and afterwards also to more complicated processes. Among the approximations for $gg \to HH$ are large top quark mass expansions [8–10], high-energy expansions [11, 12], small transverse-momentum expansions [13] and expansions around the top quark threshold [14]. In refs. [15, 16] a method has been developed where the two-loop amplitude is expanded for small Higgs boson mass with a subsequent numerical evaluation.

Since such approximations are only valid in a restricted phase space it is tempting to combine different approaches. A first example of such a combination has been presented in ref. [17] where the exact numerical results from refs. [2, 3] were combined with the high-energy expansion of refs. [11, 12]. The CPU-time expensive calculations were only necessary for relatively small values of the Higgs transverse momentum, say below $p_T \approx 200\,\text{GeV}$, and the fast evaluation of the analytic high-energy expansions could be used for the remaining phase space.

A similar approach to the one discussed in this paper has been discussed in refs. [18, 19] where the analytic small p_T and high-energy expansions are "merged". For both expansions Padé approximants are constructed, however, only to low order ([1/1] and [6/6], respectively). The Padé approximants are constructed from the analytic expression and kept fixed, thus there is no estimation of the uncertainty due to this approach. In our approach high-order Padé approximants are constructed numerically in the high-energy region and the approach of ref. [20] is used to determine an uncertainty estimate. Furthermore, instead of an expansion in p_T we perform an expansion first in the external Higgs boson mass, followed by an expansion in the (massless) Mandelstam variable t. Although both approaches are an expansion about the forward kinematics (where $q_3 = -q_1$), they differ in the terms retained in the final result; whereas refs. [18, 19] contain terms proportional to p_T and m_H in a homogenous manner, we keep all terms up to fixed maximum powers of m_H and t. Note that in [18, 19] only terms up to m_H^2 have been used in the high-energy approximation. This introduces a systematic uncertainty of up to a few percent, as we will discuss below. In this work we will include quartic corrections which reduces this uncertainty below the percent level.

JHEP06(2023)063

In this paper we review the high-energy expansion method developed in refs. [12, 17, 20]. An improvement in the method allows us to obtain significantly deeper expansions in m_t^2/s, m_t^2/t and m_t^2/u which includes terms up to about m_t^{120} (see also ref. [21]) (instead of m_t^{32} as in [12, 20]). The deeper expansions combined with the construction of Padé approximants extends the range of validity to even smaller values of $\sqrt{s}$ and p_T. We will provide details regarding this approach in section 2.1.

In section 2.2 we will describe our approach for the expansion around $t \to 0$. It is based on the observation that for this limit a simple Taylor expansion can be performed, rather than a complicated asymptotic expansion. We can thus reduce the calculation to integrals which only depend on m_t^2/s. These integrals are obtained with the help of differential equations using the "expand and match" approach developed in refs. [22, 23]. The boundary conditions are obtained from the large-m_t limit, in which the integrals are simple and can be computed analytically.

In section 3 we will use the process $gg \to HH$ to illustrate the methods of sections 2.1 and 2.2. However, the approach is more general and with straightforward modifications it can also be applied to other processes as, e.g., $gg \to ZH$. We will show that we can cover the whole kinematic phase space which we parametrize in terms of $\sqrt{s}$ and p_T. A summary of our findings together with a discussion of possible bottlenecks are discussed in section 4.

2 Analytic expansions

We begin by performing a Taylor expansion in the masses of the final-state particles. This is always possible for diagrams where the final-state particles couple to massive internal lines. This produces an amplitude in terms of four-point functions which depend on s, t and m_t, but not on m_X or m_Y. We then proceed by considering analytic expansions of the amplitude in the following limits:

A. high energy

B. $t \to 0$

In both cases we perform an exact reduction of the amplitude to master integrals, which we then expand in the relevant limit. The reduction is the same for both cases, leading to the same master integrals. For the process $gg \to HH$ this step was first done in refs. [11, 12] and leads to 161 two-loop master integrals. In the following subsections we briefly discuss the features of methods A and B in more detail.

It is also possible to perform an asymptotic expansion in the limit of a large top quark mass. In this case it is not necessary to expand in the masses of the final state particles. Such an expansion is automated in the program `exp` [24, 25] and the approach is well established; results for the $gg \to HH$ form factors at three loops can be found in refs. [9, 26]. In this work we use the results of this approach to provide boundary conditions for the differential equations considered in method B described above. We also show some numerical values for the form factors in this approximation in section 3.3, however our proposed procedure to approximate the two-loop form factors requires only the high-energy and small-t expansions.

JHEP06(2023)063

2.1 High-energy expansion

The method of high-energy expansion, including a subsequent Padé approximant–based improvement, has been developed in refs. [11, 12, 17, 20, 27]. We improve this approach by constructing a deeper expansion of the master integrals, which includes 120 terms in the small-m_t expansion. Such an expansion is obtained in the following way:

1. We insert an ansatz for the expansion of each master integral M_i, $i = 1, \ldots, 161$

$$M_i(\epsilon, s, t, m_t) = \sum_{a=-3}^{a_{i,\max}} \sum_{b=-3}^{b_{\max}} \sum_{c=0}^{4+a} c_{abc}^{(i)}(s,t)\, \epsilon^a \left(\frac{m_t}{\sqrt{s}}\right)^b \ln\left(\frac{m_t^2}{s}\right)^c , \tag{2.1}$$

   into the system of differential equations for the master integrals, with respect to m_t. $a_{i,\max}$ is a master integral–specific value determined by the ϵ order required to produce the amplitude to ϵ^0 and we choose $b_{\max} = 120$ for each master integral. The planar master integrals depend only on even powers of m_t, while the non-planar integrals also have contributions from odd powers as was shown in ref. [12].

2. By comparing the coefficients of powers of ϵ, m_t and $\ln(m_t)$ we establish a system of linear equations for the expansion coefficients $c_{abc}^{(i)}(s,t)$, which depend on the Mandelstam variables s and t. We solve this system in terms of a small number of boundary constants by making use of the `reduce_user_defined_system` feature of `Kira` [28]. Solving over finite fields with subsequent rational reconstruction using `FireFly` [29, 30] is much faster than solving symbolically using `Fermat` [31]. It is this method of solving the system of equations which allows us to expand much more deeply than ref. [12], which expands only up to $b_{\max} = 32$.

3. The boundary constants can be fixed using the solutions from refs. [11, 12], where these constants were computed using the method of regions and Mellin-Barnes techniques, see also ref. [32] for more details.

The expansion coefficients of the master integrals are then exported to a `FORM Tablebase` which is used to efficiently insert the expansions into the amplitude, which is also expanded in ϵ and m_t to the required depth.

The subsequent Padé approximation is performed numerically following refs. [17, 20]. For convenience we repeat the important steps in the following. The starting point is a form factor as an expansion in m_t, i.e., numerical values for all other kinematic variables and masses are inserted. We then apply the replacements $m_t^{2k} \to m_t^{2k} x^k$ and $m_t^{2k-1} \to m_t^{2k-1} x^k$ to pair together the even and odd powers of m_t, yielding a degree-N polynomial in the variable x, with half the maximum degree of the m_t expansion.

Next we construct Padé approximants in the variable x and write the form factor as a rational function of the form

$$[n/m](x) = \frac{a_0 + a_1 x + \ldots + a_n x^n}{1 + b_1 x + \ldots + b_m x^m} , \tag{2.2}$$

where the coefficients a_i and b_i are determined by comparing the coefficients of x^k after expanding the right-hand side of eq. (2.2) around the point $x = 0$. Evaluation of this rational function at $x = 1$ yields the Padé approximated value for the form factor.

JHEP06(2023)063

The numerator and denominator degrees (n, m) in eq. (2.2) are free parameters; one only must ensure that $n + m \leq N$ such that a sufficient number of expansion terms are available to determine the coefficients a_i and b_i. We define N_{low} and N_{high} and include Padé approximations in our analysis which fulfil

$$N_{\text{low}} \leq n + m \leq N_{\text{high}} \quad \text{and} \quad N_{\text{low}} \leq n + m - |n - m| \,. \tag{2.3}$$

Our default choice is $N_{\text{low}} = 49$ and $N_{\text{high}} = 56$ which leads to 28 different Padé approximants.[1] They are combined using three different criteria:

- The rational function in eq. (2.2) develops poles at the roots of the denominator. We give more weight to those Padé approximants which have poles further away from the evaluation point $x = 1$ ("pole-distance re-weighted" Padé approximation).
- We give more weight to Padé approximants which are derived from a larger number of expansion terms.
- We give more weight to "near-diagonal" Padé approximants.

We combine the weights from each criterion for each of the Padé approximants, and use the combined weight to produce a central value and corresponding uncertainty for the phase-space point under consideration. Explicit formulae for the individual steps of the construction are given in section 4 of ref. [20]. In the supplementary material [33] to this paper we provide `Mathematica` code which can be used to construct, for a given polynomial in x, an approximation based on the procedure described above, including an uncertainty estimate.

We have demonstrated this approach applied to a single planar master integral in ref. [21] and the comparison to (exact) numerical results can be found in figure 7(a) of that reference. In figure 2 we discuss results for the non-planar integral shown in figure 1. We choose $p_T = 40\,\text{GeV}$ and vary $\sqrt{s}$ between 300 GeV and 1100 GeV. In figure 2(a) we compare Padé results constructed from expansions up to m_t^{32} and m_t^{112}, which are shown by the green and orange bands, respectively. One observes a dramatic reduction of the uncertainty. At the same time it is reassuring to see that the uncertainty estimate of the Padé procedure is reliable, when comparing to the numerical values obtained using FIESTA [34]. In figure 2(b) we focus on the comparison of the orange band with the results from FIESTA; we observe good agreement within uncertainties in the whole plotted range of $\sqrt{s}$, even very close to the threshold for the production of two top quarks.

2.2 Expansion for $t \to 0$

In this subsection we aim for an expansion of the original 161 master integrals around $t = 0$ such that the amplitude can be expanded in this limit. This complements the high-energy expansion, i.e. we aim for a good description in the region around the threshold where $s \approx 4m_t^2$ and the high-energy expansion breaks down. However, as we will see below, good

[1] While the master integrals are determined up to $N = 60$ (m_t^{120}), negative powers of m_t in the amplitude coefficients mean that the expansion of the form factors can be produced up to $N = 56$ (m_t^{112}).

JHEP06(2023)063

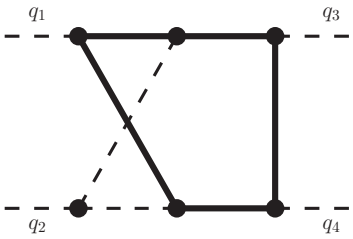

Figure 1. The two-loop Feynman diagram $G_{59}(1,1,1,1,1,1,1,-1,0)$ (see appendix A of ref. [12] for more details). Solid and dashed lines correspond to massive and massless propagators. All external momenta are massless.

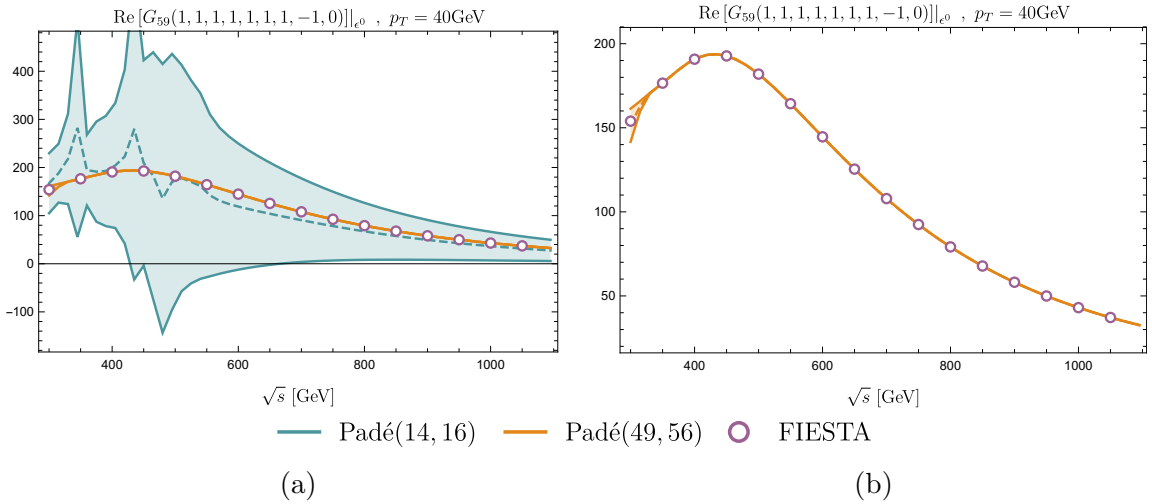

Figure 2. Comparison of Padé-based approximations constructed from different expansion depths $(N_{\text{low}}, N_{\text{high}})$ with numerical results obtained using `FIESTA`, for the non-planar master integral shown in figure 1, with a numerator.

results are also obtained for larger values of $\sqrt{s}$, in particular for smaller values of p_T. The expansion is performed as follows.

- As for the high-energy expansion, we first expand in the masses of the final-state particles. For $gg \to HH$ it is sufficient to expand up to m_H^4 to obtain a precision below the percent level. We are left with integral families which depend on s, t and m_t. Here we note that the expansion in m_H generates spurious $1/t$ terms which cancel after inserting the t-expansion of the master integrals.

  As discussed previously, this expansion is a simple Taylor expansion in cases where the final-state particles couple to massive internal lines; otherwise, a more involved asymptotic expansion must be performed.
- Establish differential equations, with respect to t, for the master integrals of the $2 \to 2$ problem where all external lines are massless. The master integrals, and thus the resulting t-differential equations, are the same as in the high-energy case discussed in section 2.1.

JHEP06(2023)063

- We use the differential equations to obtain, for each master integral, a generic Taylor expansion around $t = 0$. This is achieved by expanding the coefficients of the differential equations around $t \to 0$ and for each master integral, inserting an ansatz of the form

$$M_i(\epsilon, s, t, m_t) = \sum_{a=-3}^{a_{i,\max}} \sum_{b\geq 0} c_{ab}^{(i)}(s, m_t^2)\, \epsilon^a \left(\frac{t}{m_t^2}\right)^b ,$$

  where the (unknown) coefficients $c_{ab}^{(i)}(s, m_t^2)$ are functions of s and m_t^2.

Note that for $t \to 0$ some of the propagators of the original integral families (see appendix A of refs. [11] and [12]) become linearly dependent. After a partial fraction decomposition we can define new integral families which contain fewer propagators. In terms of these new families, the number of master integrals in the $t \to 0$ limit reduces from 161 to 48. One of the resulting topologies has been studied in ref. [35], where it was shown that two master integrals are elliptic and cannot be expressed in terms of iterated integrals. These master integrals depend on two different square roots.

We have calculated all 46 non-elliptic master integrals analytically by solving the associated differential equations in the variable s/m_t^2 following the algorithms outlined in ref. [36] implemented with the help of the packages `Sigma` [37, 38], `OreSys` [39] and `HarmonicSums` [40–52]. The boundary conditions have been fixed in the large-m_t limit, where the integrals can be calculated by performing a large mass expansion, implemented in `q2e/exp` [24, 25]. Our final result can be expressed in terms of iterated integrals over letters which contain the three square roots $\sqrt{x}\sqrt{4-x}, \sqrt{x}\sqrt{4+x}, \sqrt{4-x}\sqrt{4+x}$. However, we find that this representation is not well suited for numerical evaluation for several reasons:

1. Some of the iterated integrals depend on two square-root valued letters at the same time, which cannot easily be rationalized simultaneously.

2. The iterated integrals have spurious poles at $s/m_t^2 = 1$ and $s/m_t^2 = 4$, which require analytic continuation.

3. The analytic results for the two elliptic integrals are rather involved.

Therefore, we calculate all 48 master integrals using the semi-analytic approach developed in refs. [53, 54]. For each master integral, we provide a deep expansion of 50 terms around different values of s/m_t^2, with high-precision numerical coefficients. In particular we construct expansions around 18 values of s/m_t^2 to cover values of s between 0 and ∞. Our starting point for the construction of the approximations is the expansion around $s = 0$ where all master integrals can be computed analytically. As a by-product we extend the large-m_t expansion of these master integrals (but only at $t = 0$).

This method has a number of advantages compared to purely numerical approaches. Since the value of m_t is only inserted into the final expression, it is possible to easily change the value or renormalization scheme used for m_t. It is straightforward to take derivatives w.r.t. m_t of the one-loop expressions in order to generate the corresponding counterterm contributions.

JHEP06(2023)063

3 Application to Higgs boson pair production

In this section we apply the expansion methods discussed above to the particular case of the $gg \to HH$ amplitude. We start by examining the m_H and t expansions of one-loop master integrals by comparing to numerical results obtained with `FIESTA` [34] and `Package-X` [55]. We show that the Taylor expansion in m_H produces good agreement with the exact result, even for smaller values of $\sqrt{s}$ close to the Higgs pair production threshold at $\sqrt{s} = 2m_H$. Afterwards we discuss results for the one- and two-loop form factors. Finally we compare the virtual corrections to the Higgs pair production cross section with the numerical results obtained in ref. [17].

For the numerical evaluations we use input values for the top quark and Higgs boson masses of $m_t = 173.21\,\text{GeV}$ and $m_H = 125.1\,\text{GeV}$, respectively.

For completeness we provide in the following the definition of the form factors for Higgs boson pair production. The amplitude for the process $g(q_1)g(q_2) \to H(q_3)H(q_4)$ can be decomposed into two Lorentz structures (a and b are adjoint colour indices)

$$\mathcal{M}^{ab} = \varepsilon_{1,\mu}\varepsilon_{2,\nu}\mathcal{M}^{\mu\nu,ab} \;=\; \varepsilon_{1,\mu}\varepsilon_{2,\nu}\delta^{ab}X_0 s\,(F_1 A_1^{\mu\nu} + F_2 A_2^{\mu\nu})\,, \tag{3.1}$$

where

$$\begin{aligned} A_1^{\mu\nu} &= g^{\mu\nu} - \frac{1}{q_{12}} q_1^\nu q_2^\mu\,, \\ A_2^{\mu\nu} &= g^{\mu\nu} + \frac{1}{p_T^2 q_{12}}\left(q_{33} q_1^\nu q_2^\mu - 2q_{23} q_1^\nu q_3^\mu - 2q_{13} q_3^\nu q_2^\mu + 2q_{12} q_3^\mu q_3^\nu\right). \end{aligned} \tag{3.2}$$

Here we have introduced the abbreviation $q_{ij} = q_i \cdot q_j$ and p_T is given in eq. (1.3). The prefactor X_0 is given by

$$X_0 = \frac{G_F}{\sqrt{2}}\frac{\alpha_s(\mu)}{2\pi} T_F\,, \tag{3.3}$$

where $T_F = 1/2$, G_F is Fermi's constant and $\alpha_s(\mu)$ is the strong coupling constant evaluated at the renormalization scale μ.

We define the expansion in α_s of the form factors as

$$F = F^{(0)} + \frac{\alpha_s(\mu)}{\pi} F^{(1)} + \cdots\,, \tag{3.4}$$

and decompose the functions F_1 and F_2 introduced in eq. (3.1) into "triangle" and "box" form factors. We thus cast the one- and two-loop corrections in the form ($k = 0, 1$)

$$\begin{aligned} F_1^{(k)} &= \frac{3m_H^2}{s - m_H^2} F_{\text{tri}}^{(k)} + F_{\text{box1}}^{(k)} + \delta_{k1} F_{\text{dt1}}^{(1)}\,, \\ F_2^{(k)} &= F_{\text{box2}}^{(k)} + \delta_{k1} F_{\text{dt2}}^{(1)}\,. \end{aligned} \tag{3.5}$$

$F_{\text{dt1}}^{(1)}$ and $F_{\text{dt2}}^{(1)}$ denote the contribution from one-particle reducible double-triangle diagrams, see, e.g. figure 1(f) of ref. [17]. The main focus in this paper is on $F_{\text{box1}}^{(1)}$ and $F_{\text{box2}}^{(1)}$. Analytic results for the leading-order form factors are available from [56, 57] and the two-loop triangle form factors have been computed in refs. [58–60]. The results for the double-triangle contribution can be found in [10].

JHEP06(2023)063

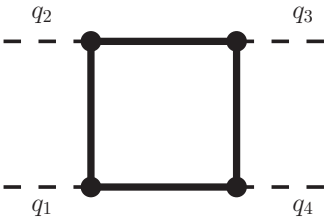

Figure 3. The one-loop master integral $G_2(1,1,1,1)$, where all internal lines are massive and for the external lines we have $q_1^2 = q_2^2 = 0$ and $q_3^2 = q_4^2 = m_H^2$.

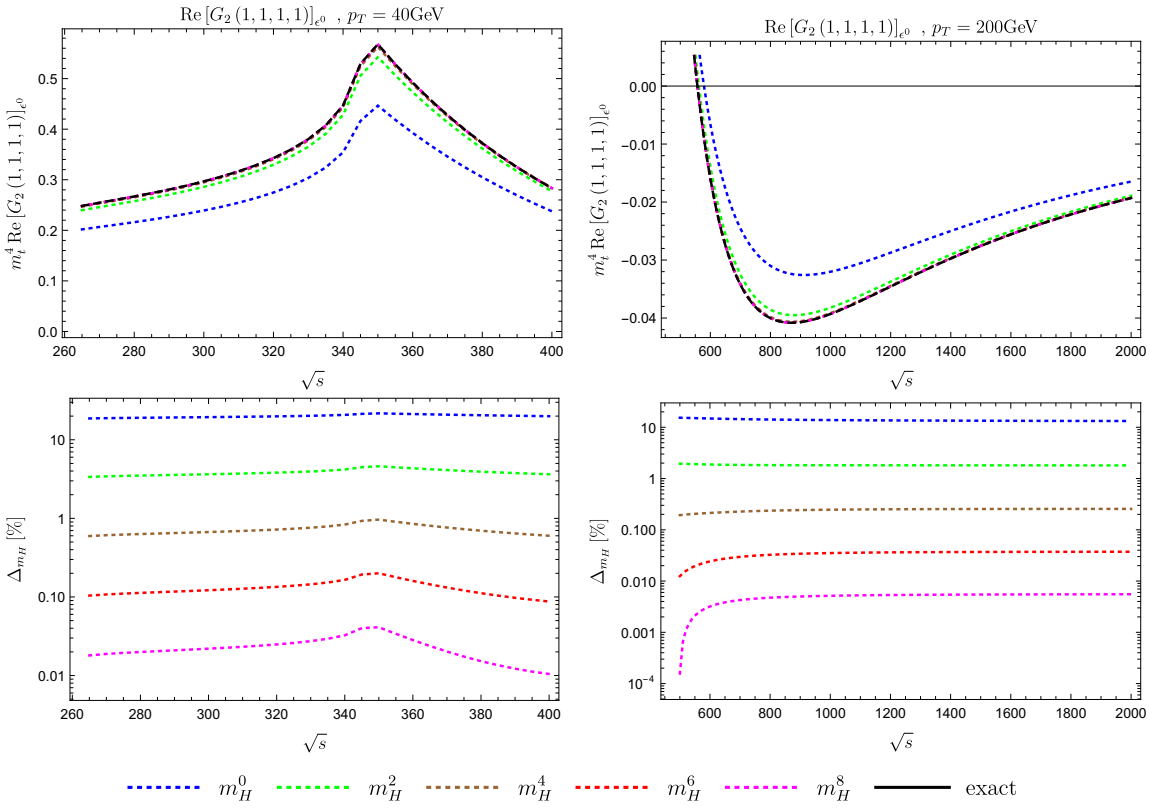

Figure 4. Real part of the master integral $G_2(1,1,1,1)$ as a function of $\sqrt{s}$ for $p_T = 40\,\mathrm{GeV}$ (left) and $p_T = 200\,\mathrm{GeV}$ (right). The coloured lines include expansions in m_H up to the indicated orders. The exact result is shown in black. The lower panels show the relative error between the expansions and the exact curve.

JHEP06(2023)063

3.1 Expansion of a one-loop master integral in m_H

In figure 4 we show, as a function of $\sqrt{s}$, the real part of the one-loop box master integral $G_2(1,1,1,1)$ (see appendix A of ref. [11] for details on the notation), which is depicted in figure 3. The left and right panels correspond to $p_T = 40\,\text{GeV}$ and $p_T = 200\,\text{GeV}$, respectively. The coloured lines show expansions in m_H^2 up to fourth order, and the black line represents the exact result. After the Taylor expansion in m_H a reduction to master integrals is necessary. It has been performed with `LiteRed` [61] and for the numerical evaluation of the resulting master integrals we have used `Package-X` [55].

The upper row shows the results for the master integral and the lower row shows the relative error between the expansions and the exact curve. One observes that the m_H^0 curves do not describe the exact result particularly well, with differences at the 15-20% level, however including the quadratic and quartic terms provide a description below the 5% level and 1% level, respectively; these observations are largely independent of the values of $\sqrt{s}$ and p_T.

3.2 Expansion of a one-loop master integral in t

Next we study the $t \to 0$ expansion of the same one-loop box master integral, $G_2(1,1,1,1)$. For this purpose we choose $m_H = 0$, i.e., the leading term of the expansion discussed in

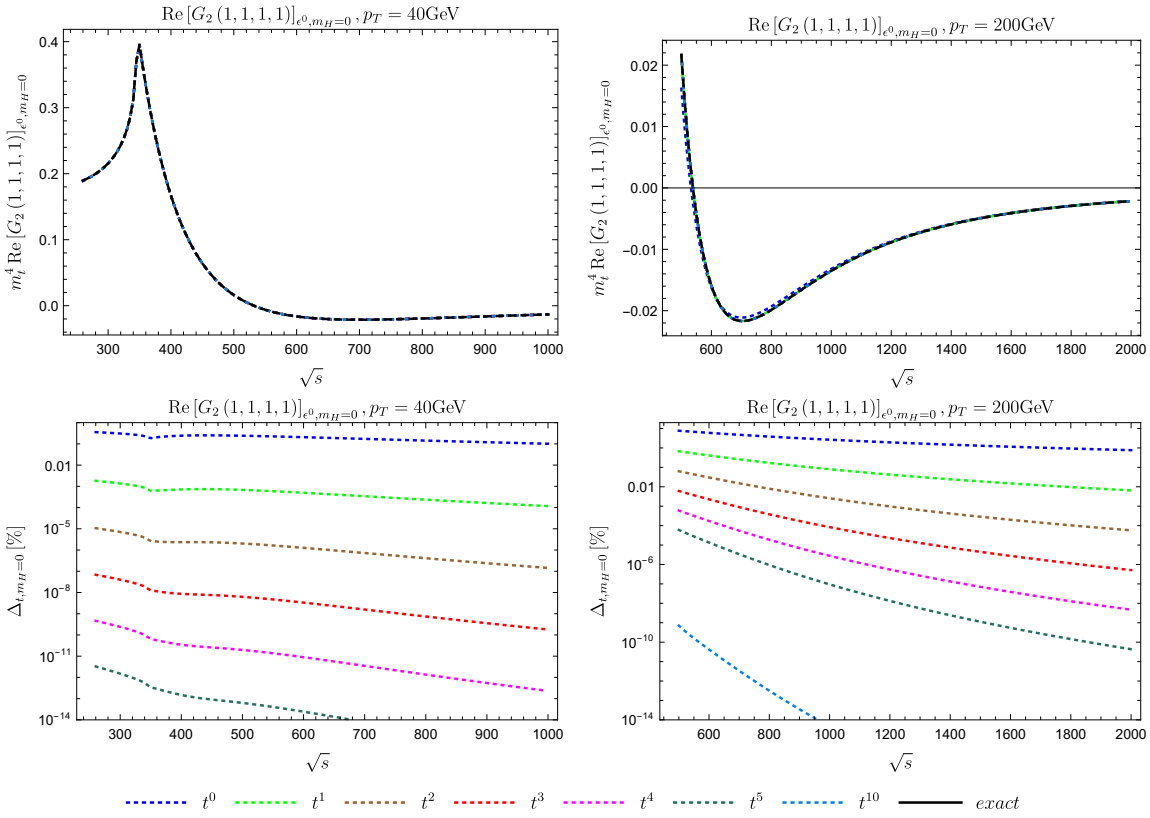

Figure 5. Real part of the master integral $G_2(1,1,1,1)$ as a function of $\sqrt{s}$ for $p_T = 40\,\text{GeV}$ (left) and $p_T = 200\,\text{GeV}$ (right). The coloured lines include expansions in t up to t^{10}. The exact result is shown in black. The lower panels show the relative error between the expansions and the exact curve.

JHEP06(2023)063

section 3.1. We perform the expansion in t using `LiteRed` [61] and then map the resulting integrals to new integral families which have only three propagators and depend only on s/m_t^2. For these integrals we establish a system of differential equations which can be solved analytically, incorporating boundary conditions from the $s \to 0$ limit. The resulting coefficients of the polynomial in t can be written in terms of Harmonic Polylogarithms [62], which we evaluate using the `Mathematica` package `HPL.m` [63, 64].

In figure 5 we show the convergence of the t expansion for the values $p_T = 40\,\text{GeV}$ and $p_T = 200\,\text{GeV}$ in the left and right columns, respectively. The lower row shows the relative error between the expansion and the exact curve. For the smaller value of $p_T = 40\,\text{GeV}$, we observe that the leading expansion term (t^0) already reproduces the exact result at the percent level. For $p_T = 200\,\text{GeV}$ the leading term does not perform so well, however by including higher-order terms the expansion converges on the exact result very quickly.

3.3 Expansion of the one-loop form factors

We now discuss the high-energy and small-t expansions at the level of the one-loop form factors $F^{(0)}_{\text{box1}}$ and $F^{(0)}_{\text{box2}}$, and compare them to the exact results.

In figures 6 and 7 we show, for various values of p_T, the results for the form factors $F^{(0)}_{\text{box1}}$ and $F^{(0)}_{\text{box2}}$ as a function of $\sqrt{s}$. The high-energy and small-t expansions are shown as coloured dashed lines; the solid black line (in the background) corresponds to the exact result. For these plots we have incorporated quartic expansion terms in m_H, the order which is also available at the two-loop level. Furthermore, for the small-t expansion terms up to t^5 are taken into account and the high-energy expansion includes Padé approximations which include terms up to at least $(m_t^2)^{49}$ and at most $(m_t^2)^{56}$.

Above the top quark pair threshold we observe that both expansions agree with the exact result even for values of p_T as small as 50 GeV and as large as 200 GeV. For larger values of p_T the small-t expansion starts to deviate from the black curve, as can be seen in the panel for $p_T = 300\,\text{GeV}$, whereas the high-energy approximation agrees very well, as expected. On the other hand, for values of p_T below 50 GeV the small-t expansion provides an excellent approximation. From the panels in figures 6 and 7 one observes that for $100\ \text{GeV} \lesssim p_T \lesssim 200\,\text{GeV}$ both approximations work well for $\sqrt{s} \gtrsim 350\,\text{GeV}$.

Below the top quark pair threshold we observe that the small-t expansion provides an excellent description of the exact result, whereas the high-energy expansion deviates; this is expected since it does not contain any information about the threshold. Values $\sqrt{s} \lesssim 2m_t$ are kinematically only allowed for $p_T \lesssim 120\,\text{GeV}$.

To quantify the quality of the approximations we show in tables 1, 2 and 3, for three different values of p_T, results for the real part of $F^{(0)}_{\text{box1}}$ for various values of $\sqrt{s}$. We show the exact results, the results for the small-t expansion for different expansion depths in m_H, the high-energy expansion including terms up to m_H^4, and results for the large-m_t expansion (LME) up to $1/m_t^{12}$ [26].

Let us start the discussion with table 1 ($p_T = 50\,\text{GeV}$) where we observe the following:

- If we restrict ourselves to the approximation which includes quartic m_H terms, in the region above the top quark threshold we observe an agreement of at least 3 significant digits between the small-t and high-energy expansions.

JHEP06(2023)063

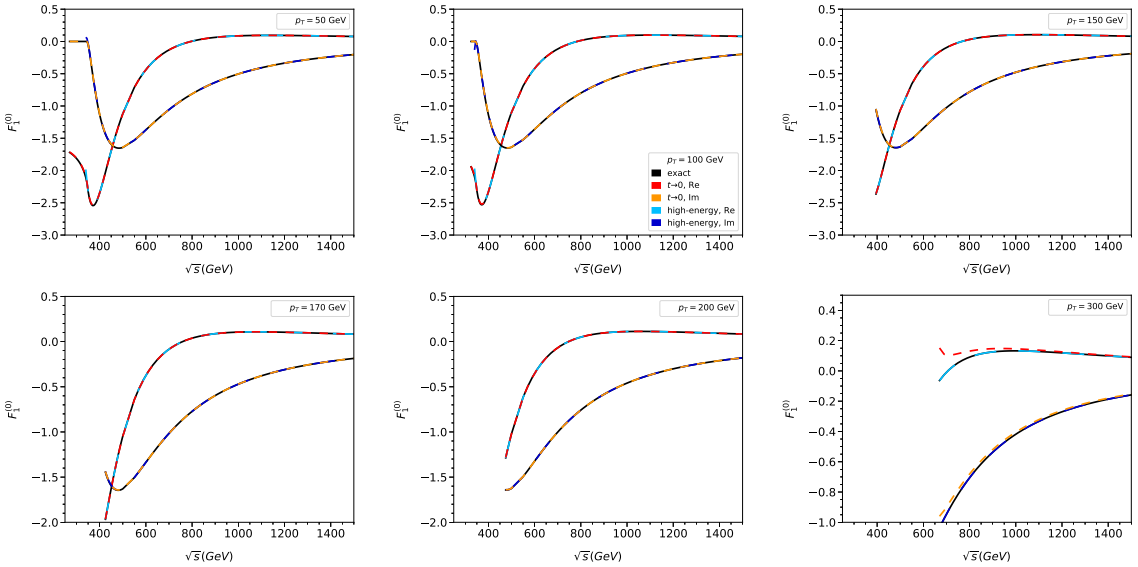

Figure 6. One-loop form factor $F^{(0)}_{\text{box1}}$ as a function of $\sqrt{s}$ for various values of p_T.

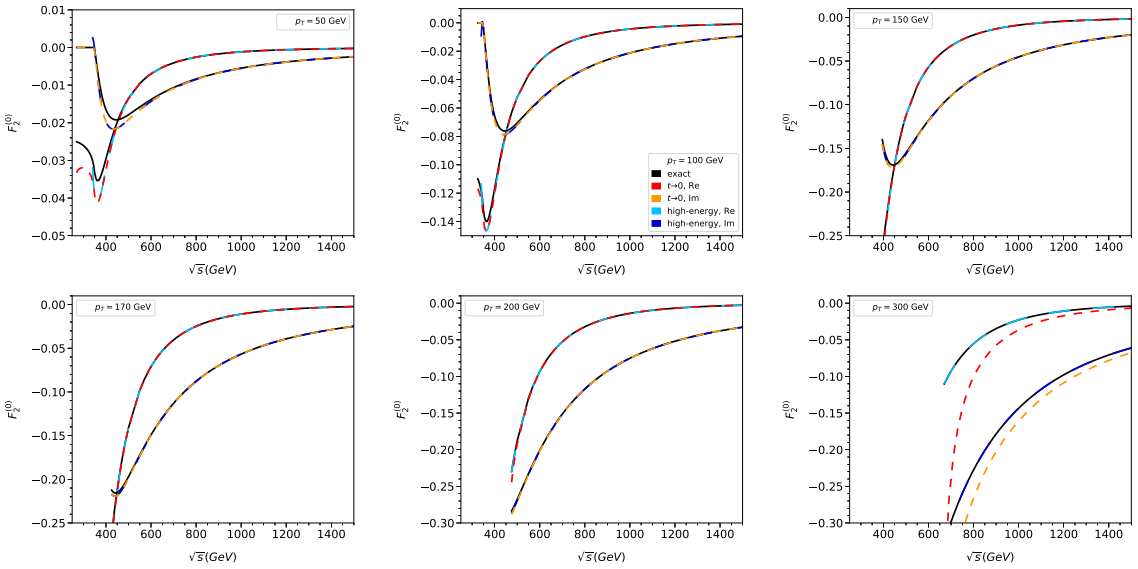

Figure 7. One-loop form factor $F^{(0)}_{\text{box2}}$ as a function of $\sqrt{s}$ for various values of p_T.

- The agreement between the exact result and the approximations based on an expansion in m_H up to quartic order is well below the percent level.

- Including expansion terms in m_H, beyond the quartic terms, for the small-t expansion improves the agreement with the exact result.

Similar conclusions also hold for $p_T = 200\,\text{GeV}$, as can be seen in table 2. In practical applications the high-energy expansion can be used for such values of p_T.

JHEP06(2023)063

$\sqrt{s}$ (GeV)		270	300	350	400	610	990
exact		−1.72013	−1.81435	−2.32246	−2.34773	−0.393996	0.0855054
small-t	m_H^0	−1.44108	−1.52523	−1.92423	−2.01154	−0.420989	0.0626770
	m_H^2	−1.67642	−1.77026	−2.25482	−2.30931	−0.404100	0.0837986
	m_H^4	−1.71321	−1.80759	−2.31050	−2.34518	−0.395265	0.0854682
	m_H^6	−1.71902	−1.81331	−2.32026	−2.34808	−0.394063	0.0855094
	m_H^8	−1.71995	−1.81419	−2.32204	−2.34793	−0.393990	0.0855057
high-en.	m_H^4	—	—	−2.31129	−2.34521	−0.395262	0.0854694
LME		−1.71813	−1.80468	−2.08865	−2.76874	—	—

Table 1. Real part of $F^{(0)}_{\text{box1}}$ for $p_T = 50\,\text{GeV}$.

In table 3 we show values for a smaller value of $p_T = 10\,\text{GeV}$. While it is impressive that for such small values of p_T the high-energy expansion still provides good approximations for $\sqrt{s}$ values around 400 GeV, which demonstrates the power of a deep expansion in m_t combined with a Padé improvement, for larger values of $\sqrt{s}$ the high-energy approximation does not reproduce the exact results. This behaviour is expected, since in this region of phase space it is not the case that $|t| \gg m_t^2$, so the high-energy expansion does not converge. Indeed for a fixed value of p_T, increasing values of $\sqrt{s}$ imply decreasing values of $|t|$. The small-t expansion performs very well in this region.

For $F^{(0)}_{\text{box2}}$ the comparison is not so straightforward, as can be seen in the first two panels of figure 7 and in table 4. We observe that the expansion in m_H does not converge sufficiently quickly for the quartic terms to provide a good description of the exact curve for $p_T \lesssim 100\,\text{GeV}$. While including terms to m_H^8 in the small-t expansion again provides good agreement, such expansion terms are not available at two loops.

We show in table 4 that below the top quark pair production threshold, the large top quark expansion of ref. [26] (including expansion terms to $1/m_t^{12}$) provides a good approximation of the exact result and can be used instead in this region. However, $F^{(0)}_{\text{box2}}$ is numerically much smaller than $F^{(0)}_{\text{box1}}$; we have verified that the use of the large top quark expansion in this region does not affect the results and conclusions of section 3.5.

From the considerations above, we propose the following selection criteria for the choice of expansion in the different regions of the $\{\sqrt{s}, p_T\}$ plane:

- Below $p_T = 150\,\text{GeV}$: use small-t expansion for all values of $\sqrt{s}$.
- For $150\,\text{GeV} \lesssim p_T \lesssim 200\,\text{GeV}$ either approximation can be used.
- Above $p_T = 200\,\text{GeV}$ use the high-energy expansion for all values of $\sqrt{s}$.

As a consequence, below $\sqrt{s} = 2m_t$ the small-t expansion is always selected. The fact that the high-energy and small-t expansions agree with each other (and with the exact result) in the region $150\,\text{GeV} \lesssim p_T \lesssim 200\,\text{GeV}$ increases our confidence in the accuracy of

JHEP06(2023)063

$\sqrt{s}$ (GeV)		610	990
exact		−0.311182	0.110469
small-t	m_H^0	−0.340443	0.089788
	m_H^2	−0.319571	0.109173
	m_H^4	−0.311692	0.110538
	m_H^6	−0.310705	0.110570
	m_H^8	−0.310651	0.110567
high-energy	m_H^4	−0.312218	0.110440

Table 2. Real part of $F^{(0)}_{\text{box1}}$ for $p_T = 200\,\text{GeV}$.

$\sqrt{s}$ (GeV)		270	300	350	400	610	990
exact		−1.72358	−1.81816	−2.32666	−2.35282	−0.400246	0.0835134
small-t	m_H^0	−1.44780	−1.52956	−1.92815	−2.01570	−0.426920	0.0605334
	m_H^2	−1.68133	−1.77444	−2.25910	−2.31430	−0.410425	0.0817808
	m_H^4	−1.71707	−1.81151	−2.31474	−2.35027	−0.401533	0.0834753
	m_H^6	−1.72257	−1.81714	−2.32446	−2.35317	−0.400314	0.0835175
	m_H^8	−1.72342	−1.81800	−2.32624	−2.35302	−0.400239	0.0835137
high-en.	m_H^4	—	—	−2.32046	−2.35382	−0.464921	−0.539285
LME		−1.72158	−1.80854	−2.09373	−2.77895	—	—

Table 3. Real part of $F^{(0)}_{\text{box1}}$ for $p_T = 10\,\text{GeV}$.

$\sqrt{s}$ (GeV)		270	300	350	400	610	990
exact		−0.025050	−0.026046	−0.033323	−0.029569	−0.006633	−0.001207
small-t	m_H^0	−0.111991	−0.072393	−0.064400	−0.050849	−0.009550	−0.001571
	m_H^2	−0.069277	−0.058082	−0.061193	−0.048812	−0.008496	−0.001339
	m_H^4	−0.033254	−0.031982	−0.039319	−0.032503	−0.006558	−0.001190
	m_H^6	−0.026450	−0.027041	−0.034525	−0.029807	−0.006603	−0.001206
	m_H^8	−0.025286	−0.026208	−0.033565	−0.029543	−0.006631	−0.001207
high-en.	m_H^4	—	—	−0.039369	−0.032504	−0.006558	−0.001189
LME		−0.024977	−0.025767	−0.028531	−0.034309	—	—

Table 4. Real part of $F^{(0)}_{\text{box2}}$ for $p_T = 50\,\text{GeV}$.

the expansions; we will check for this agreement at two loops, where no exact analytic result for the form factors is available.

Finally, in tables 5 and 6 we show the convergence properties of the small-t expansion for $F^{(0)}_{\text{box1}}$, expanded to m_H^4. In table 5 we have chosen $p_T = 50\,\text{GeV}$, as in table 1.

JHEP06(2023)063

$\sqrt{s}$		270	300	350	400	610	990
exact		−1.72013	−1.81435	−2.32246	−2.34773	−0.393996	0.0855054
small-t	t^0	−1.72233	−1.81614	−2.31848	−2.35377	−0.403541	0.0831798
	t^1	−1.70636	−1.80585	−2.30978	−2.34471	−0.395059	0.0855148
	t^2	−1.71349	−1.80764	−2.31052	−2.34519	−0.395270	0.0854672
	t^3	−1.71313	−1.80758	−2.31050	−2.34518	−0.395265	0.0854682
	t^4	−1.71322	−1.80759	−2.31050	−2.34518	−0.395265	0.0854682
	t^5	−1.71321	−1.80759	−2.31050	−2.34518	−0.395265	0.0854682

Table 5. Real part of $F^{(0)}_{\text{box1}}$ for $p_T = 50\,\text{GeV}$. Note that the difference between the converged small-t expansion and the exact result is due to the limited expansion depth in m_H^2.

$\sqrt{s}$		610	990
exact		−0.271746	0.121508
small-t	t^0	−0.403541	0.083180
	t^1	−0.169798	0.140533
	t^2	−0.329867	0.111809
	t^3	−0.235303	0.126569
	t^4	−0.296885	0.118770
	t^5	−0.256537	0.122940

Table 6. Real part of $F^{(0)}_{\text{box1}}$ for $p_T = 250\,\text{GeV}$.

Here we observe a rapid convergence; in fact, the $\mathcal{O}(t^2)$ terms already provide only a small correction. For larger values of p_T the higher-order expansion terms become more important. For example, for $p_T = 250\,\text{GeV}$ (table 6) even the t^4 and t^5 terms provide important contributions.

3.4 Two-loop form factors

In the following we present results for the two-loop box form factors where for the ultraviolet renormalization and infra-red subtraction we follow ref. [12]. In particular, we renormalize the top quark mass in the on-shell scheme.

In figures 8, 9, 10 and 11 we show the results for the two colour factors of the two-loop form factors, for various values of p_T, as a function of $\sqrt{s}$. For the small-t expansion terms up to t^5 are taken into account and the high-energy expansion includes Padé approximations with at least $(m_t^2)^{49}$ and at most $(m_t^2)^{56}$ terms. In all cases quartic terms in m_H are included. Results for the high-energy form factors at the deeper expansion depths considered here are provided in the supplementary material of this paper (and also in ref. [33]).

JHEP06(2023)063

An exact result for the form factors is not at our disposal, however, we observe that the approximations show a very similar behaviour as at one-loop order. In particular, we observe that for $100\,\text{GeV} \lesssim p_T \lesssim 200\,\text{GeV}$ there is a wide range in $\sqrt{s}$ where we find excellent agreement between the two approximations. We want to stress that for these p_T values the small-t expansion works well even for larger values of $\sqrt{s}$. This is demonstrated by the black and gray curves which show the relative percentage difference between the small-t and high-energy expansions for the real and imaginary parts of the form factors, respectively. For each value of $100\,\text{GeV} \lesssim p_T \lesssim 170\,\text{GeV}$ there is an overlap region in which the relative difference is far below 1%, and mostly even below 0.1%. Note that the spikes in the gray and black curves are related to zeros of the form factors.

For $p_T > 200\,\text{GeV}$ we can rely on the high-energy expansion. This is supported by the fact that even for $p_T \approx 100\,\text{GeV}$ the high-energy expansion agrees with the small-t expansion even for $\sqrt{s} \approx 2m_t$. Note that for $\sqrt{s} < 2m_t$ the high-energy expansion is not valid for any value of p_T since no information about the top quark pair threshold is used for the construction of the approximation. However, for $\sqrt{s} < 2m_t$ the small-t approximation is always valid since p_T is kinematically constrained to be less than about 120 GeV.

For smaller values of p_T the small-t expansion is even more reliable, as can been seen from the one-loop comparison in table 3.

In summary, in sections 2.1 and 2.2 we demonstrate that the combination of the small-t and high-energy expansions is sufficient to cover the whole phase space, and that the final uncertainty is given only by the expansion in m_H which we estimate to be below 1%.

Our expressions retain explicit dependence on all parameters, (m_t, m_H, s and t), allowing for a straightforward change of parameter values or renormalization scheme. Our reference implementation of the approximations in `Mathematica` requires a few seconds to evaluate the small-t expansion and between 40 and 50 seconds to evaluate the $(m_t^2)^{56}$ Padé-improved high-energy approximation. We have also implemented both the small-t and an $(m_t^2)^{24}$ Padé-improved high-energy approximation in `C++` which requires only $\mathcal{O}(10)$ ms per phase-space point, which is comparable to the timings reported in ref. [19].

3.5 Virtual NLO corrections

As a final comparison, we construct the infra-red subtracted virtual corrections, following ref. [65]. They are given by

$$\widetilde{\mathcal{V}}_{\text{fin}} = \frac{\alpha_s^2(\mu)}{16\pi^2}\frac{G_F^2 s^2}{64}\left[C + 2\left(\tilde{F}_1^{(0)*}\tilde{F}_1^{(1)} + \tilde{F}_2^{(0)*}\tilde{F}_2^{(1)} + \tilde{F}_1^{(0)}\tilde{F}_1^{(1)*} + \tilde{F}_2^{(0)}\tilde{F}_2^{(1)*}\right)\right], \tag{3.6}$$

with

$$C = \left[\left|\tilde{F}_1^{(0)}\right|^2 + \left|\tilde{F}_2^{(0)}\right|^2\right]\left(C_A\pi^2 - C_A\log^2\frac{\mu^2}{s}\right), \tag{3.7}$$

where α_s corresponds to the five-flavour strong coupling constant. It is convenient to introduce the α_s-independent quantity

$$\mathcal{V}_{\text{fin}} = \frac{\widetilde{\mathcal{V}}_{\text{fin}}}{\alpha_s^2(\mu)}. \tag{3.8}$$

JHEP06(2023)063

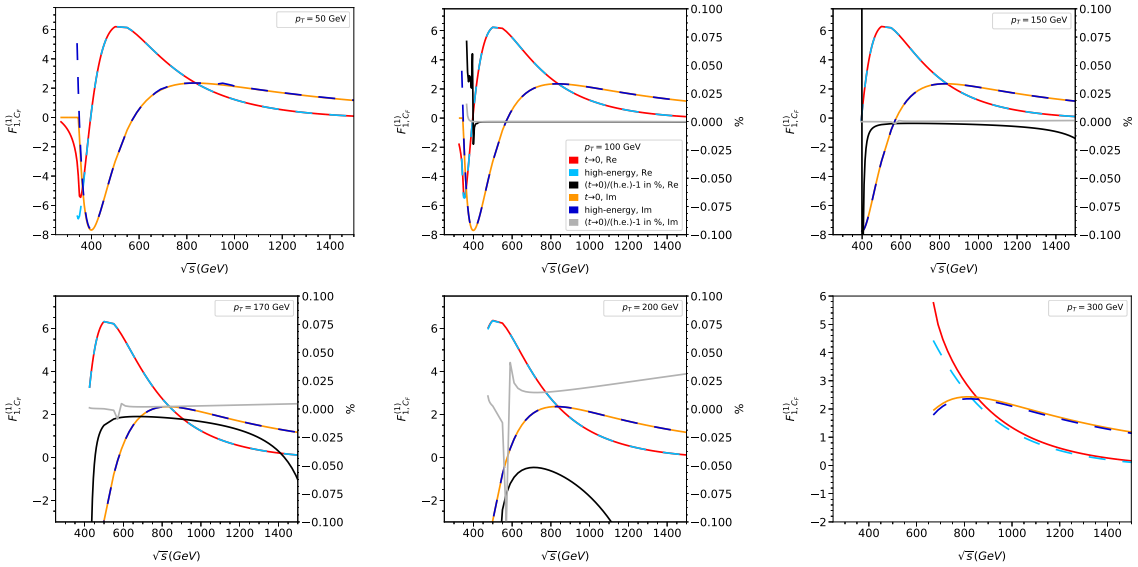

Figure 8. C_F contribution to the two-loop form factor $F^{(1)}_{\text{box1}}$ as a function of $\sqrt{s}$ for various values of p_T.

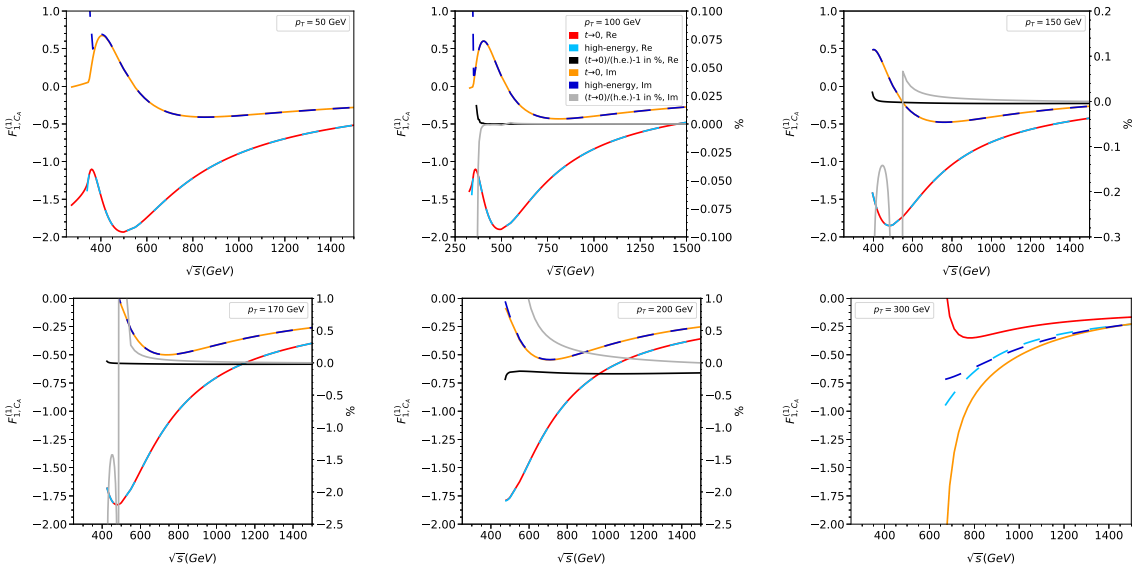

Figure 9. C_A contribution to the two-loop form factor $F^{(1)}_{\text{box1}}$ as a function of $\sqrt{s}$ for various values of p_T.

JHEP06(2023)063

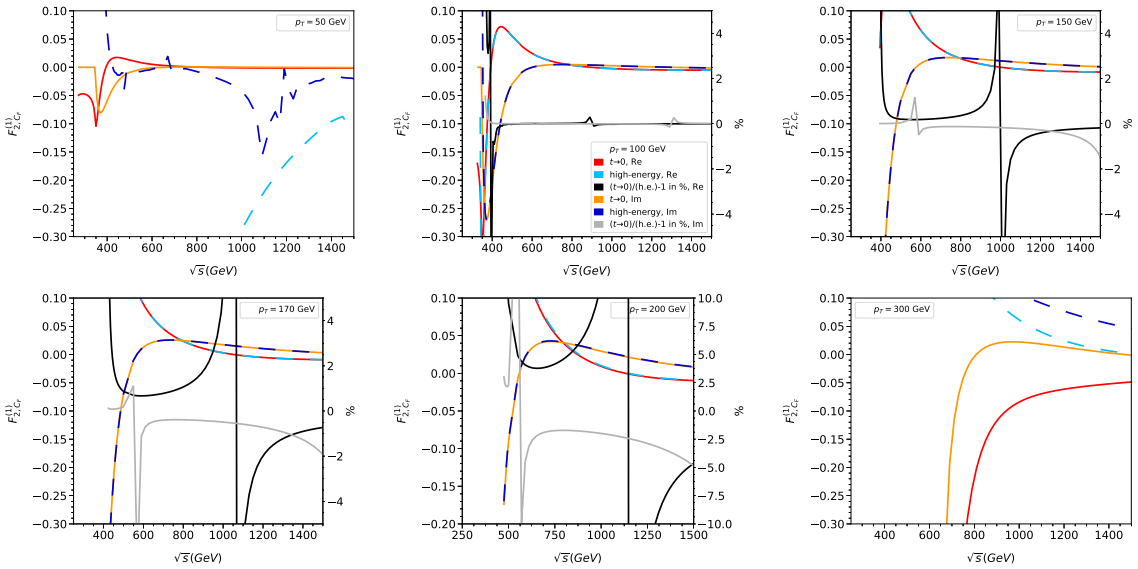

Figure 10. C_F contribution to the two-loop form factor $F^{(1)}_{\text{box2}}$ as a function of $\sqrt{s}$ for various values of p_T.

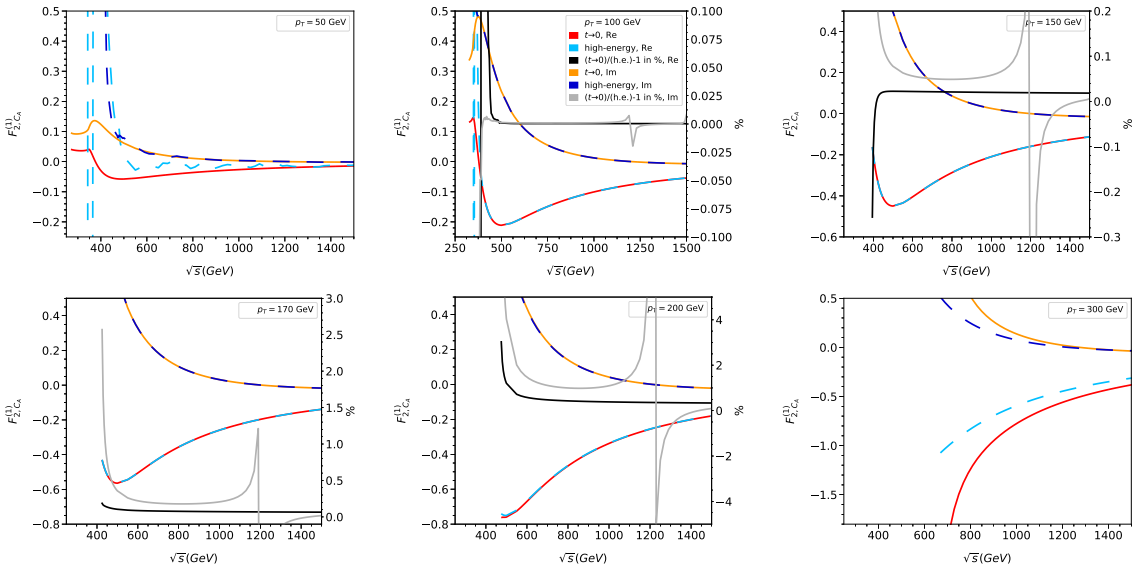

Figure 11. C_A contribution to the two-loop form factor $F^{(1)}_{\text{box2}}$ as a function of $\sqrt{s}$ for various values of p_T.

JHEP06(2023)063

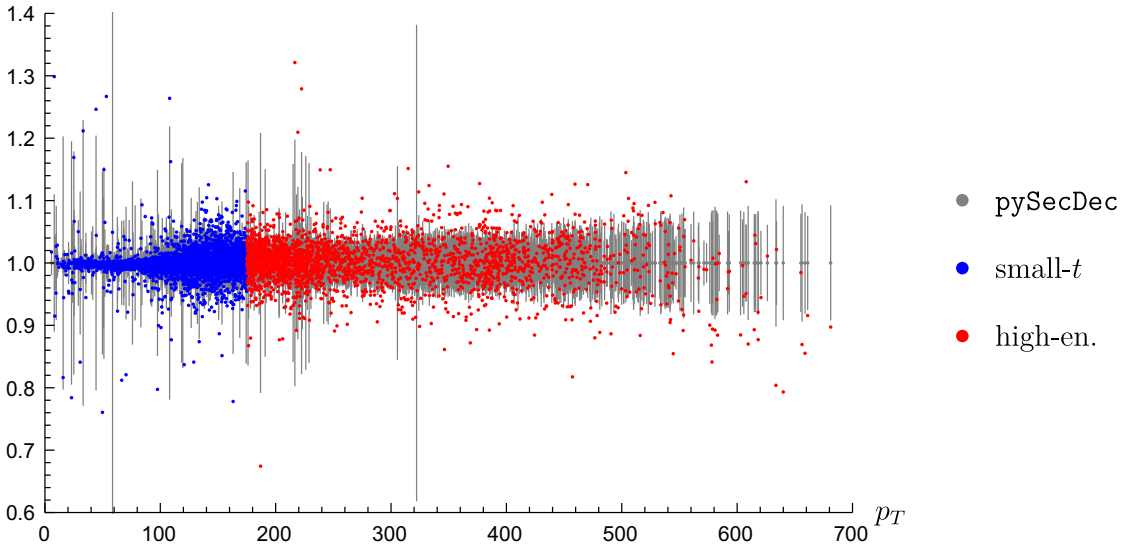

Figure 12. $\mathcal{V}_{\text{fin}}$ as a function of p_T, normalized to the central values of the `pySecDec`-evaluated points of `hhgrid`. We switch from the small-t to the high-energy expansion at $p_T = 175\,\text{GeV}$.

We use the exact expressions for the one-loop form factors along with the approximations discussed in the previous section for the two-loop form factors, to compute $\mathcal{V}_{\text{fin}}$. The triangle and double-triangle diagrams are included in the form factors, as described in eq. (3.5); we use exact expressions for the double-triangle diagrams, while for the triangle diagrams we use the expansions discussed above.

In ref. [17] the high-energy expansions of refs. [11, 12, 32] have been combined with the exact, numerical two-loop results of [65], such that $\mathcal{V}_{\text{fin}}$ can be evaluated at any phase-space point and costly two-loop numerical integrations are only required in a restricted phase space, namely for $p_T < 150\,\text{GeV}$ if $\sqrt{s} \geq 700\,\text{GeV}$ and for $p_T < 200\,\text{GeV}$ if $\sqrt{s} < 700\,\text{GeV}$. The results of [17] are collected as data points in `hhgrid` [66]. The high-energy expansion used in [17] only includes terms up to m_t^{32}, in contrast to the much deeper expansions which we consider in this work.

In figure 12 we compare our new results for $\mathcal{V}_{\text{fin}}$ to those obtained using `pySecDec` [67, 68] in ref. [17]. The grey data points and uncertainties correspond to the `pySecDec` data points, normalized to their central values. In comparison the uncertainty of our approximation is negligible.[2] The blue and red data points are obtained from the small-t and high-energy expansions, where we normalize to the central values of the `hhgrid` data. This plot may be compared with figure 3 of ref. [17].

To quantify the agreement between our approximations and the `pySecDec` evaluations, the following table describes the proportion of points which are contained within a number of `pySecDec` error intervals.

[2]The systematic uncertainty of about 1% due to the expansion in m_H up to quartic order is not shown.

JHEP06(2023)063

pySecDec err. intervals	1σ	2σ	3σ
small-t	0.57	0.85	0.92
high-energy	0.65	0.94	0.99

We observe that the high-energy expansion demonstrates a Gaussian behaviour, while the small-t expansion shows a non-Gaussian disagreement, which we ascribe to the systematic error due to the slower convergence of the m_H^2 expansion in the lower-p_T region, as shown in figure 4.

Let us finally compare to the findings of refs. [18, 19]. In these works the integration over t has been performed and an uncertainty of 1% is claimed with respect to the exact LO values. Here we present detailed results only at the level of the form factors, and find a several-digit agreement between our small-t and high-energy approximations in the overlap region for p_T between 100 GeV and 200 GeV. On the other hand, the results for the form factors in ref. [18] suggest a several-percent difference between the two Padé-improved expansions in some cases, as shown in figures 1 and 3 of ref. [18]; the form factor with the worse agreement (F_{box2}) only has a small contribution to the cross section, however.

In refs. [18, 19] only 13 high-energy terms have been taken into account to construct a [6/6] Padé approximant and thus the transition from the small-p_T to the high-energy approximation is made at relatively high values of p_T ($p_T \approx 312\,\text{GeV}$ and 340 GeV for the choices $\sqrt{s} = 900\,\text{GeV}$ and $\sqrt{s} = 2000\,\text{GeV}$ in figure 3 of ref. [18]). As we show in figures 6 and 7 our small-t expansion does not perform very well in this region. However in our approach, we are able to use the high-energy expansion at much smaller values of p_T, so this region is well described. Let us also mention that in refs. [18, 19] only quadratic m_H terms are used in the high-energy expansion which leads to a few-percent systematic uncertainty at the level of the form factors.

In the small-p_T expansion in refs. [18, 19] only a [1/1] Padé approximant is constructed which means that three expansion terms are available. In our analysis we use terms up to t^5, i.e. six expansion terms; no Padé improvement of the $t \to 0$ expansion is necessary. We have shown in table 6 that the deeper expansion terms are important to approximate higher p_T values without the use of Padé approximants.

4 Conclusions

In this paper we consider a $2 \to 2$ process with massive internal particles, which is a multi-scale problem and thus notoriously difficult, both in an analytic and in a numerical approach. We show that the combination of analytic expansions in two regions of phase space provides a complete description of the two-loop virtual amplitude. On the one hand we consider a deep expansion in the high-energy limit where the internal mass (in our application, the top quark mass) is small compared to the Mandelstam variables s and t. On the other hand we perform an expansion in t which again eliminates a scale from the integrand. In both cases we expand in the mass of the final-state particles.

We discuss in detail the two-loop corrections for $gg \to HH$ and show that for this process no numerical integration is necessary to obtain the differential virtual corrections. Other processes such as $gg \to ZH$ or $gg \to ZZ$ can be treated in analogy.

JHEP06(2023)063

Using a similar approach to the one applied in this paper it might be possible to extend the $t \to 0$ expansion to three loops, yielding the NNLO virtual corrections to this gluon fusion processes. Possible bottlenecks, which have to be studied in the future, are huge intermediate expressions and the integration-by-parts reduction of the expanded amplitudes to master integrals.

Acknowledgments

We would like to thanks Gudrun Heinrich and Stephen Jones for helpful comments on the draft of this manuscript. This research was supported by the Deutsche Forschungsgemeinschaft (DFG, German Research Foundation) under grant 396021762 — TRR 257 "Particle Physics Phenomenology after the Higgs Discovery" and has received funding from the European Research Council (ERC) under the European Union's Horizon 2020 research and innovation programme grant agreement 101019620 (ERC Advanced Grant TOPUP). The work of GM was supported by JSPS KAKENHI (No. JP20J00328). The work of JD was supported by the Science and Technology Facilities Council (STFC) under the Consolidated Grant ST/T00102X/1.

References

[1] F. Maltoni, E. Vryonidou and M. Zaro, *Top-quark mass effects in double and triple Higgs production in gluon-gluon fusion at NLO*, *JHEP* **11** (2014) 079 [arXiv:1408.6542] [INSPIRE].

[2] S. Borowka et al., *Higgs boson pair production in gluon fusion at next-to-leading order with full top-quark mass dependence*, *Phys. Rev. Lett.* **117** (2016) 012001 [*Erratum ibid.* **117** (2016) 079901] [arXiv:1604.06447] [INSPIRE].

[3] S. Borowka et al., *Full top quark mass dependence in Higgs boson pair production at NLO*, *JHEP* **10** (2016) 107 [arXiv:1608.04798] [INSPIRE].

[4] J. Baglio et al., *Gluon fusion into Higgs pairs at NLO QCD and the top mass scheme*, *Eur. Phys. J. C* **79** (2019) 459 [arXiv:1811.05692] [INSPIRE].

[5] B. Agarwal, S.P. Jones and A. von Manteuffel, *Two-loop helicity amplitudes for $gg \to ZZ$ with full top-quark mass effects*, *JHEP* **05** (2021) 256 [arXiv:2011.15113] [INSPIRE].

[6] L. Chen et al., *ZH production in gluon fusion: two-loop amplitudes with full top quark mass dependence*, *JHEP* **03** (2021) 125 [arXiv:2011.12325] [INSPIRE].

[7] C. Brønnum-Hansen and C.-Y. Wang, *Two-loop helicity amplitudes for W/Z boson pair production in gluon fusion with exact top mass dependence*, *JHEP* **05** (2021) 244 [arXiv:2101.12095] [INSPIRE].

[8] S. Dawson, S. Dittmaier and M. Spira, *Neutral Higgs boson pair production at hadron colliders: QCD corrections*, *Phys. Rev. D* **58** (1998) 115012 [hep-ph/9805244] [INSPIRE].

JHEP06(2023)063

[9] J. Grigo, J. Hoff, K. Melnikov and M. Steinhauser, *On the Higgs boson pair production at the LHC*, *Nucl. Phys. B* **875** (2013) 1 [arXiv:1305.7340] [INSPIRE].

[10] G. Degrassi, P.P. Giardino and R. Gröber, *On the two-loop virtual QCD corrections to Higgs boson pair production in the standard model*, *Eur. Phys. J. C* **76** (2016) 411 [arXiv:1603.00385] [INSPIRE].

[11] J. Davies, G. Mishima, M. Steinhauser and D. Wellmann, *Double-Higgs boson production in the high-energy limit: planar master integrals*, *JHEP* **03** (2018) 048 [arXiv:1801.09696] [INSPIRE].

[12] J. Davies, G. Mishima, M. Steinhauser and D. Wellmann, *Double Higgs boson production at NLO in the high-energy limit: complete analytic results*, *JHEP* **01** (2019) 176 [arXiv:1811.05489] [INSPIRE].

[13] R. Bonciani, G. Degrassi, P.P. Giardino and R. Gröber, *Analytical method for next-to-leading-order QCD corrections to double-Higgs production*, *Phys. Rev. Lett.* **121** (2018) 162003 [arXiv:1806.11564] [INSPIRE].

[14] R. Gröber, A. Maier and T. Rauh, *Reconstruction of top-quark mass effects in Higgs pair production and other gluon-fusion processes*, *JHEP* **03** (2018) 020 [arXiv:1709.07799] [INSPIRE].

[15] X. Xu and L.L. Yang, *Towards a new approximation for pair-production and associated-production of the Higgs boson*, *JHEP* **01** (2019) 211 [arXiv:1810.12002] [INSPIRE].

[16] G. Wang et al., *Efficient computation of two-loop amplitudes for Higgs boson pair production*, *Phys. Rev. D* **104** (2021) L051901 [arXiv:2010.15649] [INSPIRE].

[17] J. Davies et al., *Double Higgs boson production at NLO: combining the exact numerical result and high-energy expansion*, *JHEP* **11** (2019) 024 [arXiv:1907.06408] [INSPIRE].

[18] L. Bellafronte et al., *Gluon fusion production at NLO: merging the transverse momentum and the high-energy expansions*, *JHEP* **07** (2022) 069 [arXiv:2202.12157] [INSPIRE].

[19] G. Degrassi, R. Gröber, M. Vitti and X. Zhao, *On the NLO QCD corrections to gluon-initiated ZH production*, *JHEP* **08** (2022) 009 [arXiv:2205.02769] [INSPIRE].

[20] J. Davies, G. Mishima, M. Steinhauser and D. Wellmann, *$gg \to ZZ$: analytic two-loop results for the low- and high-energy regions*, *JHEP* **04** (2020) 024 [arXiv:2002.05558] [INSPIRE].

[21] J. Davies et al., *Higgs boson contribution to the leading two-loop Yukawa corrections to $gg \to HH$*, *JHEP* **08** (2022) 259 [arXiv:2207.02587] [INSPIRE].

[22] M. Fael, F. Lange, K. Schönwald and M. Steinhauser, *A semi-numerical method for one-scale problems applied to the $\overline{\text{MS}}$-on-shell relation*, *SciPost Phys. Proc.* **7** (2022) 041 [arXiv:2110.03699] [INSPIRE].

[23] M. Fael, F. Lange, K. Schönwald and M. Steinhauser, *Singlet and nonsinglet three-loop massive form factors*, *Phys. Rev. D* **106** (2022) 034029 [arXiv:2207.00027] [INSPIRE].

[24] T. Seidensticker, *Automatic application of successive asymptotic expansions of Feynman diagrams*, in the proceedings of the 6th *International workshop on new computing techniques in physics research: software engineering, artificial intelligence neural nets, genetic algorithms, symbolic algebra, automatic calculation*, (1999) [hep-ph/9905298] [INSPIRE].

JHEP06(2023)063

[25] R. Harlander, T. Seidensticker and M. Steinhauser, *Complete corrections of $O(\alpha\alpha_s)$ to the decay of the Z boson into bottom quarks*, *Phys. Lett. B* **426** (1998) 125 [hep-ph/9712228] [INSPIRE].

[26] J. Davies and M. Steinhauser, *Three-loop form factors for Higgs boson pair production in the large top mass limit*, *JHEP* **10** (2019) 166 [arXiv:1909.01361] [INSPIRE].

[27] J. Davies, G. Mishima and M. Steinhauser, *Virtual corrections to $gg \to ZH$ in the high-energy and large-m_t limits*, *JHEP* **03** (2021) 034 [arXiv:2011.12314] [INSPIRE].

[28] J. Klappert, F. Lange, P. Maierhöfer and J. Usovitsch, *Integral reduction with Kira* 2.0 *and finite field methods*, *Comput. Phys. Commun.* **266** (2021) 108024 [arXiv:2008.06494] [INSPIRE].

[29] J. Klappert, S.Y. Klein and F. Lange, *Interpolation of dense and sparse rational functions and other improvements in FireFly*, *Comput. Phys. Commun.* **264** (2021) 107968 [arXiv:2004.01463] [INSPIRE].

[30] J. Klappert and F. Lange, *Reconstructing rational functions with FireFly*, *Comput. Phys. Commun.* **247** (2020) 106951 [arXiv:1904.00009] [INSPIRE].

[31] R.H. Lewis, *Fermat's user guide*, http://home.bway.net/lewis/.

[32] G. Mishima, *High-energy expansion of two-loop massive four-point diagrams*, *JHEP* **02** (2019) 080 [arXiv:1812.04373] [INSPIRE].

[33] J. Davies, G. Mishima, K. Schoenwald and M. Steinhauser, *Analytic approximations of $2 \to 2$ processes with massive internal particles — supplementary material*, https://www.ttp.kit.edu/preprints/2023/ttp23-004/.

[34] A.V. Smirnov, N.D. Shapurov and L.I. Vysotsky, *FIESTA5: numerical high-performance Feynman integral evaluation*, *Comput. Phys. Commun.* **277** (2022) 108386 [arXiv:2110.11660] [INSPIRE].

[35] A. von Manteuffel and L. Tancredi, *A non-planar two-loop three-point function beyond multiple polylogarithms*, *JHEP* **06** (2017) 127 [arXiv:1701.05905] [INSPIRE].

[36] J. Ablinger et al., *Automated solution of first order factorizable systems of differential equations in one variable*, *Nucl. Phys. B* **939** (2019) 253 [arXiv:1810.12261] [INSPIRE].

[37] C. Schneider, *Symbolic summation assists combinatorics*, *Sém. Lothar. Combin.* **56** (2007) 1.

[38] C. Schneider and J. Blümlein, *Computer algebra in quantum field theory. Integration, summation and special functions*, in *Proceedings, LHCPhenoNet school: Linz, Austria,* 9–13 *July* 2012, (2013) [DOI:10.1007/978-3-7091-1616-6] [INSPIRE].

[39] S. Gerhold, *Uncoupling systems of linear Ore operator equations*, Diploma Thesis, RISC, J. Kepler University, Linz, Austria (2002).

[40] J.A.M. Vermaseren, *Harmonic sums, Mellin transforms and integrals*, *Int. J. Mod. Phys. A* **14** (1999) 2037 [hep-ph/9806280] [INSPIRE].

[41] J. Blümlein, *Structural relations of harmonic sums and Mellin transforms up to weight $w = 5$*, *Comput. Phys. Commun.* **180** (2009) 2218 [arXiv:0901.3106] [INSPIRE].

[42] J. Ablinger, *A computer algebra toolbox for harmonic sums related to particle physics*, M.Sc. thesis, Linz U., Linz, Austria (2009) [arXiv:1011.1176] [INSPIRE].

[43] J. Ablinger, J. Blümlein and C. Schneider, *Harmonic sums and polylogarithms generated by cyclotomic polynomials*, *J. Math. Phys.* **52** (2011) 102301 [arXiv:1105.6063] [INSPIRE].

JHEP06(2023)063

[44] J. Ablinger, J. Blümlein and C. Schneider, *Analytic and algorithmic aspects of generalized harmonic sums and polylogarithms*, *J. Math. Phys.* **54** (2013) 082301 [arXiv:1302.0378] [INSPIRE].

[45] J. Ablinger, *Computer algebra algorithms for special functions in particle physics*, Ph.D. thesis, Linz U., Linz, Austria (2012) [arXiv:1305.0687] [INSPIRE].

[46] J. Ablinger, J. Blümlein and C. Schneider, *Generalized harmonic, cyclotomic, and binomial sums, their polylogarithms and special numbers*, *J. Phys. Conf. Ser.* **523** (2014) 012060 [arXiv:1310.5645] [INSPIRE].

[47] J. Ablinger, J. Blümlein, C.G. Raab and C. Schneider, *Iterated binomial sums and their associated iterated integrals*, *J. Math. Phys.* **55** (2014) 112301 [arXiv:1407.1822] [INSPIRE].

[48] J. Ablinger, *The package HarmonicSums: computer algebra and analytic aspects of nested sums*, *PoS* **LL2014** (2014) 019 [arXiv:1407.6180] [INSPIRE].

[49] J. Ablinger, *Inverse Mellin transform of holonomic sequences*, arXiv:1606.02845.

[50] J. Ablinger, *Computing the inverse Mellin transform of holonomic sequences using Kovacic's algorithm*, *PoS* **RADCOR2017** (2018) 001 [arXiv:1801.01039] [INSPIRE].

[51] J. Ablinger, *An improved method to compute the inverse Mellin transform of holonomic sequences*, *PoS* **LL2018** (2018) 063 [INSPIRE].

[52] J. Ablinger, *Discovering and proving infinite Pochhammer sum identities*, arXiv:1902.11001 [INSPIRE].

[53] M. Fael, F. Lange, K. Schönwald and M. Steinhauser, *A semi-analytic method to compute Feynman integrals applied to four-loop corrections to the* $\overline{\text{MS}}$*-pole quark mass relation*, *JHEP* **09** (2021) 152 [arXiv:2106.05296] [INSPIRE].

[54] M. Fael, F. Lange, K. Schönwald and M. Steinhauser, *Massive vector form factors to three loops*, *Phys. Rev. Lett.* **128** (2022) 172003 [arXiv:2202.05276] [INSPIRE].

[55] H.H. Patel, *Package-X* 2.0*: a Mathematica package for the analytic calculation of one-loop integrals*, *Comput. Phys. Commun.* **218** (2017) 66 [arXiv:1612.00009] [INSPIRE].

[56] E.W.N. Glover and J.J. van der Bij, *Higgs boson pair production via gluon fusion*, *Nucl. Phys. B* **309** (1988) 282 [INSPIRE].

[57] T. Plehn, M. Spira and P.M. Zerwas, *Pair production of neutral Higgs particles in gluon-gluon collisions*, *Nucl. Phys. B* **479** (1996) 46 [*Erratum ibid.* **531** (1998) 655] [hep-ph/9603205] [INSPIRE].

[58] R. Harlander and P. Kant, *Higgs production and decay: analytic results at next-to-leading order QCD*, *JHEP* **12** (2005) 015 [hep-ph/0509189] [INSPIRE].

[59] C. Anastasiou et al., *Two-loop amplitudes and master integrals for the production of a Higgs boson via a massive quark and a scalar-quark loop*, *JHEP* **01** (2007) 082 [hep-ph/0611236] [INSPIRE].

[60] U. Aglietti, R. Bonciani, G. Degrassi and A. Vicini, *Analytic results for virtual QCD corrections to Higgs production and decay*, *JHEP* **01** (2007) 021 [hep-ph/0611266] [INSPIRE].

[61] R.N. Lee, *LiteRed* 1.4*: a powerful tool for reduction of multiloop integrals*, *J. Phys. Conf. Ser.* **523** (2014) 012059 [arXiv:1310.1145] [INSPIRE].

[62] E. Remiddi and J.A.M. Vermaseren, *Harmonic polylogarithms*, *Int. J. Mod. Phys. A* **15** (2000) 725 [hep-ph/9905237] [INSPIRE].

JHEP06(2023)063

[63] D. Maitre, *HPL, a Mathematica implementation of the harmonic polylogarithms*, *Comput. Phys. Commun.* **174** (2006) 222 [hep-ph/0507152] [INSPIRE].

[64] D. Maitre, *Extension of HPL to complex arguments*, *Comput. Phys. Commun.* **183** (2012) 846 [hep-ph/0703052] [INSPIRE].

[65] G. Heinrich et al., *NLO predictions for Higgs boson pair production with full top quark mass dependence matched to parton showers*, *JHEP* **08** (2017) 088 [arXiv:1703.09252] [INSPIRE].

[66] *hhgrid GitHub webpage*, https://github.com/mppmu/hhgrid.

[67] S. Borowka et al., *pySecDec: a toolbox for the numerical evaluation of multi-scale integrals*, *Comput. Phys. Commun.* **222** (2018) 313 [arXiv:1703.09692] [INSPIRE].

[68] S. Borowka et al., *A GPU compatible quasi-Monte Carlo integrator interfaced to pySecDec*, *Comput. Phys. Commun.* **240** (2019) 120 [arXiv:1811.11720] [INSPIRE].

JHEP06(2023)063